

Frequency division multiplexing readout of 60 low-noise transition-edge sensor bolometers

Wang, Q.; Khosropanah, P.; Van Der Kuur, J.; De Lange, G.; Audley, M. D.; Aminaei, A.; Ridder, M. L.; Van Der Linden, A. J.; Bruijn, M. P.; Gao, J. R.

DOI

[10.1063/5.0065570](https://doi.org/10.1063/5.0065570)

Publication date

2021

Document Version

Accepted author manuscript

Published in

Applied Physics Letters

Citation (APA)

Wang, Q., Khosropanah, P., Van Der Kuur, J., De Lange, G., Audley, M. D., Aminaei, A., Ridder, M. L., Van Der Linden, A. J., Bruijn, M. P., & Gao, J. R. (2021). Frequency division multiplexing readout of 60 low-noise transition-edge sensor bolometers. *Applied Physics Letters*, 119(18), Article 182602. <https://doi.org/10.1063/5.0065570>

Important note

To cite this publication, please use the final published version (if applicable). Please check the document version above.

Copyright

Other than for strictly personal use, it is not permitted to download, forward or distribute the text or part of it, without the consent of the author(s) and/or copyright holder(s), unless the work is under an open content license such as Creative Commons.

Takedown policy

Please contact us and provide details if you believe this document breaches copyrights. We will remove access to the work immediately and investigate your claim.

Frequency division multiplexing readout of 60 low-noise transition-edge sensor bolometers

Frequency division multiplexing readout of 60 low-noise transition-edge sensor bolometers

Q. Wang,^{1,2,a)} P. Khosropanah,¹ J. van der Kuur,¹ G. de Lange,¹ M. D. Audley,¹ A. Aminaei,¹ M. L. Ridder,¹ A.J. van der Linden,¹ M. P. Bruijn,¹ F. van der Tak,^{1,2} and J.R. Gao^{1,3}

¹⁾*SRON Netherlands Institute for Space Research, Landleven 12, 9747 AD Groningen and Niels Bohrweg 4, 2333 CA Leiden, The Netherlands*

²⁾*Kapteyn Astronomical Institute, University of Groningen, 9747 AD Groningen, The Netherlands*

³⁾*Optics Group, Department of Imaging Physics, Delft University of Technology, 2628 CJ Delft, The Netherlands*

(Dated: 19 September 2021)

We demonstrate multiplexing readout of 60 transition edge sensor (TES) bolometers operating at 90 mK using a Frequency Division Multiplexing readout chain with bias frequencies ranging from 1 to 3.5 MHz and with a typical frequency spacing of 32 kHz. The readout chain starts with a two-stage SQUID amplifier and has a noise level of $9.5 \text{ pA}/\sqrt{\text{Hz}}$. We compare the current-voltage curves and noise spectra of the TESs measured in single-pixel mode and in multiplexing mode. We also map the noise equivalent power (NEP) and the saturation power of the bolometers in both modes, where there are 43 pixels that show not more than 10% difference in NEP and 5% in saturation power when measured in single pixel and multiplex mode. We have read out a TES with an NEP of $0.45 \text{ aW}/\sqrt{\text{Hz}}$ in the multiplexing-mode, which demonstrates the capability of reading out ultra-low noise TES bolometer arrays for space applications.

Frequency division multiplexing (FDM) is one of the most promising techniques for the read-out of transition edge sensor (TES) bolometers arrays¹⁻³. The FDM readout technique has the advantage of being able to bias each TES in the array individually for optimum settings and shows a competitive performance⁴ compared to other promising readout techniques such as the time division multiplexing (TDM)⁵ and the microwave superconducting quantum interference device (SQUID) readout^{6,7}. FDM techniques are currently being developed for ground-based observatories^{8,9}, balloon-borne observatories^{10,11} and considered for space observatories, such as Lite satellite for the studies of B-mode polarization and Inflation from cosmic background Radiation Detection (LiteBIRD)¹² and the far-infrared spectrometer (SAFARI) proposed for the recently cancelled Space Infrared Telescope for Cosmology and Astrophysics (SPICA)^{13,14}. The spacecraft platforms usually have limited resources of power, mass and volume^{4,13} which could restrict the use of the ground based FDM technology. The requirements of SAFARI, for example, not only impose a different configuration of the FDM readout chain than that of the ground-based system, but also demand different LC filter designs, e.g., small frequency spacing and a compact chip design¹⁵.

An FDM system suitable for space platforms has three key requirements: (a) it requires a higher multiplexing factor, i.e. a narrow frequency spacing between two adjacent pixels, determined by the array of LC filters¹⁶, and a small number of readout chains. The latter decreases the dissipation power from the SQUID amplifiers and the readout electronics, and also the complexity of the system¹⁶; (b) the noise level of the readout must be lower than that of the TES detectors, implying noise current spectral density $(A/\sqrt{\text{Hz}}) S_{I,read}$

$< \sqrt{S_{I,ph}^2 + S_{I,Jo}^2}$, where $S_{I,read}$ is the current noise level in the SQUID input, while $S_{I,ph}$ and $S_{I,Jo}$ are the phonon noise and Johnson noise of the detectors, respectively³; (c) the crosstalk between detectors should be sufficiently low¹⁷, i.e., the measured characteristics of a TES, which are read out in a multiplexing mode (MM), namely measuring several bolometers simultaneously, should be the same as when read out in a single-pixel mode (SPM). The SPM is well calibrated and has no crosstalk issue.

The required noise equivalent power (NEP) of TES bolometers for SAFARI is $0.2 \text{ aW}/\sqrt{\text{Hz}}$. The challenge of a low NEP readout system is to satisfy the requirements on crosstalk while adding minimal noise. Bolometers with the required NEP have already been realized: a single pixel TES was reported with an NEP as low as $0.1 \text{ aW}/\sqrt{\text{Hz}}$ ¹⁸. The state of the art of the FDM technology is reported in reference⁹, where 206 pixels were successfully read out with six SQUID amplifiers with an NEP of $\sim 30 \text{ aW}/\sqrt{\text{Hz}}$. Another work that reported 176-pixel FDM readout system suffered from high readout noise and crosstalk¹⁹. Until now, a low readout noise FDM system suitable for readout of multiple pixels with a low NEP ($\leq 0.2 \text{ aW}/\sqrt{\text{Hz}}$) has not been demonstrated.

In this letter, we report simultaneous readout of 60 low NEP TES bolometers using an FDM readout demonstrator, with a nominal frequency spacing of 32 kHz and a low readout noise level of $9.5 \text{ pA}/\sqrt{\text{Hz}}$. The TES array contains detectors with various sensitivities, which allow us to demonstrate the FDM for detectors with different NEPs down to $0.45 \text{ aW}/\sqrt{\text{Hz}}$. Our focus is to compare the performance of TES bolometers when they are operated in SPM or MM.

Fig.1 shows the cold electronics part of our FDM demonstrator that contains a TES array of 176-pixels, two LC filter chips with 88 resonators each, and SQUID amplifiers. Both the TES array and the filter chips are exactly the same as used in our previous work to address the crosstalk¹⁷. Coplanar wiring lines connect all the bolometers on the detec-

^{a)}Author to whom correspondence should be addressed: Q.Wang@sron.nl

This is the author's peer reviewed, accepted manuscript. However, the online version of record will be different from this version once it has been copyedited and typeset.

PLEASE CITE THIS ARTICLE AS DOI: 10.1063/5.0065570

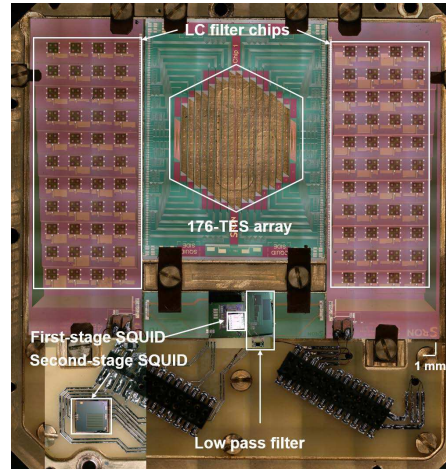


FIG. 1. Photo of the cold electronics part of an FDM readout demonstrator with two SQUID chips at the bottom. One half array of 88-pixels is connected to one of the LC filter chips. An RC (resistor-capacitor) low pass filter is introduced to eliminate the out-of-band resonance peaks.

tor array chip for easy fabrication, while microstrip lines are used on the LC filter chips and to connect the LC filter chip to the SQUID for low mutual inductance. Nowadays microstrip lines are also used for TES arrays. All the wire bonds are Aluminum, which is superconducting at the operating temperature. All parts are mounted inside a copper sample enclosure, which is physically closed, but has been found not to be fully light-tight based on the results in¹⁸. An adiabatic demagnetization refrigerator (ADR)¹⁷ is used to cool down the enclosure. Our measurements were performed at 90 mK and the background magnetic field of the TES was nulled by applying a magnetic field using a Helmholtz coil¹⁷. In practice, we cannot finish all measurements within one cool-down cycle. Therefore, due to the instability of the cooling power and the presence of 50-Hz noise between two cooling cycles, we observed a maximum 5% and 10% measurement error in current-voltage (IV) curve and noise spectrum, respectively.

Compared to our setup described in reference¹⁷ we have changed the SQUID amplifier and added a resistor-capacitor low-pass filter (LPF), both of which are operated at the bath temperature. The decoupled two-stage SQUID amplifier²⁰ decreases the readout noise, minimizes the common inductance that is due to inductive coupling of the SQUID, and eliminates the back-action effect²¹. The latter refers to a phenomenon where the feedback noise is added to the input signal. Applying the SQUID calibration tone method described in²², we measured the readout noise to be $9.5 \text{ pA}/\sqrt{\text{Hz}}$, a factor of 2.5 lower than the readout noise reported in reference²², which focuses on SPM. The LPF has a cut off frequency of 7 MHz, and is introduced to minimize the unwanted out of band reso-

nance peaks at 20 MHz and 100 MHz. The series resistance in the circuit when the TES is superconducting is $1.9 \pm 0.3 \text{ m}\Omega$, which comprises the shunt resistance ($1 \text{ m}\Omega$) and a parasitic resistance. The common inductance in the SQUID input coil is $\leq 3 \text{ nH}$. The details of the warm electronics can be found in reference²³, while a diagram of FDM system is also available in the supplementary materials.

We connect half of the TES array to one of the LC filter chips with resonance frequencies ranging from 1 to 3.5 MHz, and frequency spacing of $32 \pm 3 \text{ kHz}$. 60 out of 88 resonators had Q-factors $\geq 10^4$ and were therefore chosen for our FDM experiment. Other pixels either had resonator Q-factor that was too low or an unusable TES, due to defects in the Si_3N_4 legs or issues with wire bonds.

The bolometers are made from $50 \times 50 \text{ }\mu\text{m}^2$ Ti/Au ($16/65 \text{ nm}$) TESs connected to $100 \times 100 \text{ }\mu\text{m}^2$ Ta absorbers that are 9 nm thick and suspended on top of a 250-nm-thick Si_3N_4 membrane island using four 400- μm -long 2- μm wide Si_3N_4 legs. More device parameters can be found in reference¹⁷. For this experiment, we measured the DC normal resistance (R_n) of some pixels (pixels 1, 17, 29, 58) in the array separately and found it to be $200 \pm 10 \text{ m}\Omega$. We also found the critical temperature (T_c) of the TESs to be $113 \pm 3 \text{ mK}$ and to be relatively constant within the array. The latter is found by fitting the measured saturation power (P_{sat}) of the TESs at different operating temperatures.

An NEP of $0.7 \text{ aW}/\sqrt{\text{Hz}}$ is expected from the nominal values of the designed T_c (100 mK) and thermal conductance (G ; 0.8 pW/K). However, by performing IV measurements at different bath temperatures we found that G varies from 0.16 to 1.10 pW/K , a factor of 6.8. These data were taken from seven pixels across the entire bias frequency range. The variation in G could not be explained by deviations in the width of the legs since they are found to be constant and close to the nominal value. Therefore we attribute the variation in G to the wet-etching process^{24,25} used to fabricate the TESs.

Before addressing the properties of the 60 pixels from the array, we focus first on one pixel, i.e. pixel 29, as an example, operated at a biasing frequency of 2.2 MHz. Fig.2 shows comparisons of the detector characteristics measured in either SPM or MM. The calibrated IV curves of pixel 29 are shown in Fig.2 (a) and are essentially same in the two modes. However, there is a small deviation ($< 5\%$) between the two modes when the TES is biased at a low voltage ($\leq 25 \text{ nV}$), which corresponds to a relatively low part of the transition region ($R_{TES}/R_n < 20\%$) and does not affect detector operation in practice. Fig.2 (b) shows the observed P_{sat} at different bias points along the resistive transition, measured in both modes. The P_{sat} at 90 mK is 7.83 fW in SPM and 7.93 fW in MM, with a relative difference of only 1.2%. Thus they agree within the measurement error. The inset of Fig.2 (b) shows a fit of measured P_{sat} at different bath temperatures in SPM to the equation, $P_{sat} = K(T_c^n - T_{bath}^n)$ ²⁶, for the power flow to the bath, where K is a scaling parameter for the heat flux and n is a factor reflecting the thermal characteristics of the legs, which ranges from 2 to 4 (2.5 for this pixel). G is found to be 0.43 pW/K , derived from the expression: $G = dP/dT = nKT_c^{(n-1)}$, where the T_c is 113 mK. Now, the phonon noise limited NEP,

This is the author's peer reviewed, accepted manuscript. However, the online version of record will be different from this version once it has been copyedited and typeset.

PLEASE CITE THIS ARTICLE AS DOI: 10.1063/1.50065570

Frequency division multiplexing readout of 60 low-noise transition-edge sensor bolometers

3

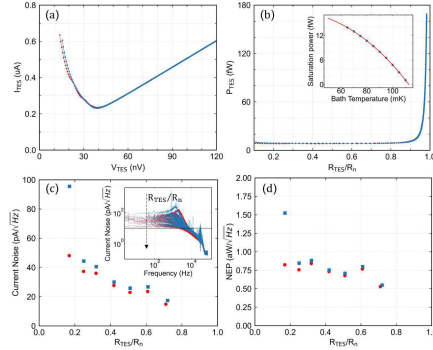


FIG. 2. (a) IV characteristics of a TES bolometer (pixel 29) in SPM (dashed lines in red) and MM (solid lines in blue). (b) P_{sat} at different transition points, R_{TES}/R_n , compared in SPM and MM. The inset of (b) is the power plateau fit with P_{sat} measured at different operating temperatures. (c) Current noise spectra in SPM (red filled circles) and MM (blue filled squares). Inset in (c): Current noise spectra in SPM and MM. The constant line indicates the readout noise level of $9.5 \text{ pA}/\sqrt{\text{Hz}}$; (d) NEP plot at different transition points measured in SPM and MM. There is a significant difference in the first data point between SPM and MM because the noise increases due to oscillations in MM when the TES is biased in $R_{TES}/R_n \sim 0.17$.

which is given by $\sqrt{4\gamma k_B G T_c^2}$, with $\gamma \sim 1$ (for our case according to reference²⁶) and k_B being Boltzmann's constant, is estimated to be $0.54 \text{ aW}/\sqrt{\text{Hz}}$.

The inset in Fig.2 (c) shows the full current-noise spectra of pixel 29 at various bias points in SPM and MM. When the detector is biased low in the transition, there can be oscillations that appear in the noise spectra because the TES response time ($\tau_{eff} \sim C/\alpha G \approx 0.2 \text{ ms}$) is too close to that of the readout electronics ($\tau_{el} \sim L/R_{TES} \approx 0.17 \text{ ms}$), causing an underdamped response. Fig. 2 (c) plots the average current noise values between 20 and 200 Hz at bias points in the range $R_{TES}/R_n = 17\%$ to 71% in both modes. We notice that the measured current noise levels are the same in both modes except for bias points low on the transition ($R_{TES}/R_n < 25\%$), in good agreement with what we observed in the IV curves. When pixel 29 is biased below 25% in transition, the time constant of this pixel is comparable to the electrical response time constant. In MM, a small current leakage decreases the bias voltage of this pixel, and thus may cause oscillations and raise the current noise level.

Fig.2 (d) shows the NEP versus bias point, derived from the average current noise values from Fig.2 (c) after subtracting the readout noise. Here the NEP is calculated by dividing the current noise by the responsivity of $1/V_{TES}$, where V_{TES} is the TES bias voltage. We found that the differences in NEP between SPM and MM are small and less than 10% except for the data at the low bias of $R_{TES}/R_n \leq 25\%$. The latter are expected from the corresponding current noise. The data at the bias of 51% for R_{TES}/R_n shows that the NEP is $0.72 \text{ aW}/\sqrt{\text{Hz}}$ in SPM and $0.79 \text{ aW}/\sqrt{\text{Hz}}$ in MM with a difference of 0.07

$\text{aW}/\sqrt{\text{Hz}}$. We noticed that the NEP either in SPM or MM is higher than the phonon noise limited NEP of $0.54 \text{ aW}/\sqrt{\text{Hz}}$, as given earlier. The difference is likely due to the excess noise²⁶ and photon noise in the setup, to be discussed later. We also find a clear drop of NEP at $R_{TES}/R_n = 71\%$ in the same figure. In this case the NEP is underestimated due to the use of the responsivity of $1/V_{TES}$, which is not applicable at the high bias points. The correct way to estimate the responsivity uses the expression, $(1/V_{TES})(1 + (1 + \beta)/\zeta)^{-1}$, where β is the current responsivity and ζ the loop gain²⁶. At a bias of 71% or higher, as the bias increases, ζ decreases and approaches 1, while β approaches 0, so the responsivity can be no less than half of the value used at $R_{TES}/R_n < 70\%$. As will be mentioned later, this underestimation contributes to the scattering of measured NEPs in the array.

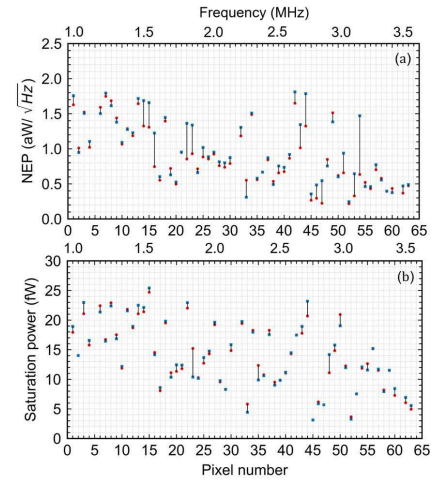


FIG. 3. (a) Measured NEPs of 60 TES pixels in both SPM (filled circles in red) and MM (filled squares in blue), where the abscissa in the bottom panel is the pixel number, while that in the top panel is the bias frequency for the pixel. The black lines between two squares indicate the differences measured between two modes. (b) Measured P_{sat} of 60 pixels in both SPM and MM.

Next, we measured the properties of the full array. The NEP and P_{sat} of all 60-pixels, biased in the frequency range from 1 to 3.5 MHz and measured in both SPM and MM, are shown in Fig.3 (a) and (b), respectively. We found the NEPs to be in a range between 0.3 and $1.8 \text{ aW}/\sqrt{\text{Hz}}$ among the 60 pixels, while P_{sat} varies from 2 to 25 fW . 20 out of these 60 pixels could not be biased below $R_{TES}/R_n = 70\%$, due to oscillations. Therefore, the NEP values of these pixels have been underestimated in both SPM and MM by the same factor.

The key result of our study is presented in Fig.4, which shows a detailed comparison of the NEP and P_{sat} of 60 pixels measured in SPM and MM according to the layout of TES pixels in the array.

We found that 43 pixels out of 60 have shown a differ-

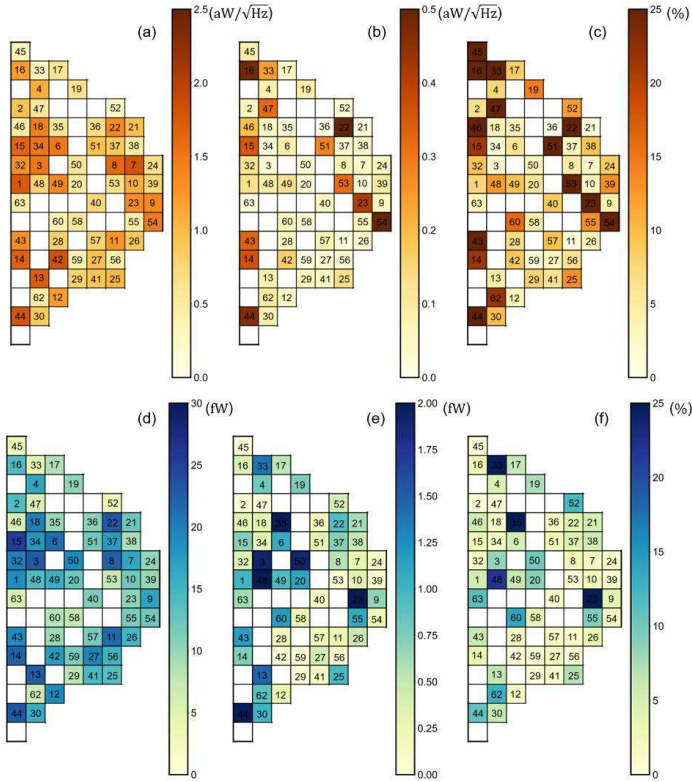


FIG. 4. (a) Map of NEP according to the layout of the TES array, measured in MM. The number inside each square denotes the pixel number; (b) Mapped differences of the NEPs between SPM and MM; (c) Mapped differences of NEP in percentage between single-pixel and multiplexing modes derived from (b) with respect to the NEP in (a); (d) Mapped P_{sat} according to the layout of TES array in the MM; (e) P_{sat} differences measured between the two modes. (f) Map of percentage differences of the P_{sat} between the two modes.

ence of not more than 10% in NEPs and 5% in P_{sat} between SPM and MM. Both of these differences could be calibrated out by measuring the response of the detectors to a known optical source²⁷. These results show that our FDM demonstrator is able to measure multiple bolometers simultaneously. Among these 43 pixels, one pixel (pixel 56) has an NEP of $0.45 \text{ aW}/\sqrt{\text{Hz}}$. This low NEP was confirmed by a separate analysis using the full expression in reference²⁶ for the NEP, using α , β from the measured complex impedance²⁸ and other parameters (e.g. T_c , G) of the pixel. The latter gives a NEP of $0.43 \text{ aW}/\sqrt{\text{Hz}}$. This particular result thus suggests our FDM is able to read out a low NEP level, approaching the requirement for SAFARI ($\sim 0.2 \text{ aW}/\sqrt{\text{Hz}}$).

There are 17 pixels that show more than 10% difference in the measured NEPs between SPM and MM, and even up to 78% in the worst case, while the difference in P_{sat} is near zero or much less significant. The large differences in NEPs

are caused by high crosstalk, previously discovered and characterized in those pixels¹⁷. Pixels 15, 16, 33, 43-47, and 53 (nine pixels in total) have high crosstalk due to carrier leakage and to mutual inductance in the co-planar wires, which could be minimized by microstrip wiring¹⁷. Pixels 14, 22, 23 and 31 (four pixels) are biased at the edge of oscillations, i.e. the TES time constant is comparable to the electrical response time constant. In this case, a small current leakage will decrease the bias voltage of those pixels, which in turn causes oscillations and raises the current noise level. Pixels 51, 54, 60 and 62 (four pixels) are operated at the higher bias frequencies and have a narrow frequency spacing of $\sim 26 \text{ kHz}$. This narrower frequency spacing could lead to higher carrier leakage, thus increasing the measured NEP.

We noticed a large variation in the measured NEPs and P_{sat} among the 60 pixels. The known variations in G from a limited number of tested pixels can cause the phonon-noise dom-

inated NEPs to vary at least from 0.3 to 0.9 aW/\sqrt{Hz} . This range becomes larger if we include the influence of the excess noise²⁹. Furthermore, there are two other mechanisms that can increase the variation in NEP. First, the photon noise due to optical loading from non-uniformly distributed stray light can increase NEPs. The stray light can also lead to the underestimation of G . However, the latter should be a small effect because of limited loading power²⁵. Second, the NEPs of the pixels that could not be biased lower than 70% in the transition can be underestimated. A further discussion is beyond the scope of this letter.

In conclusion, we have demonstrated a low noise FDM system to read out 60 TES pixels of an array by comparing the NEPs and P_{sat} measured in single-pixel mode and multiplexing mode. The readout noise is below the noise from the detectors. We find 43 of 60 pixels to have a difference in NEPs of less than or equal to 10% and a difference in the saturation power is $\leq 5\%$, both of which are within the measurement error range. For these 43 pixels, the low NEP is 0.45 aW/\sqrt{Hz} . The other 17 pixels show large differences in NEPs between the single-pixel mode and multiplexing mode that is due to the high crosstalk level. To advance the demonstrator to an FDM system that satisfies the requirements for space applications like SAFARI, we need to produce an array with slower and lower-NEP TES bolometers ($\leq 0.2 aW/\sqrt{Hz}$) and perform the measurement in a fully light-tight setup. Furthermore, we expect to be able to use our readout system up to 5 MHz^4 , which enables a multiplexing factor of ≥ 130 .

SUPPLEMENTARY MATERIAL

See the supplementary materials for a diagram of FDM readout system, parameters of the devices in FDM, and power consumption of warm electronics.

We acknowledge M. Kiviranta at VTT for providing the two-stage SQUIDS, E. Taralli and K. Ravensberg for running the ADR cooler. This work benefits greatly from the knowledge and existing hardware from a long development history of the FDM technology contributed by many people at SRON, including R. Hijmering, R. den Hartog, L. Gottardi, H. Akamatsu, D. Vaccaro, B. Jackson, P. de Korte, D. Boersma, B. van Leeuwen, J. Nieuwenhuizen, and S. Ilyas. Q.W. thanks J.G. bij de Vaate for supporting his Ph. D activity within the Instrument Science Group at SRON. Q.W. is funded partly by the China Scholarship Council (CSC) and partly by the University of Groningen.

The authors have no conflicts to disclose.

The data that support the findings of this study are available from the corresponding author upon reasonable request.

¹T. M. Lanting, H. M. Cho, J. Clarke, W. L. Holzapfel, A. T. Lee, M. Lueker, P. L. Richards, M. A. Dobbs, H. Spieler, and A. Smith, *Appl. Phys. Lett.* **86**, 112511 (2005).

²M. A. Dobbs, M. Lueker, K. Aird, A. Bender, L. Bleem, J. Carlstrom, C. Chang, H. M. Cho, J. Clarke, T. Crawford, A. Crites, D. Flanigan, T. Haan, E. George, N. Halverson, W. Holzapfel, J. Hrubes, B. Johnson, and R. Williamson, *Rev. Sci. Instrum.* **83**, 073113 (2012).

³B. D. Jackson, P. de Korte, J. van der Kuur, P. Mauskopf, J. Beyer, M. Bruijn, A. Cros, J. R. Gao, D. Griffin, R. den Hartog, M. Kiviranta,

G. de Lange, B. J. van Leeuwen, C. Macculi, L. Ravera, N. Trappea, H. van Weers, and S. Withington, *IEEE Trans. Terahertz Sci. Technol.* **2**, 12 (2012).

⁴L. Gottardi and K. Nagayashi, *Appl. Sci.* **11**, 3793 (2021).

⁵W. B. Doriese, J. A. Beall, S. Deiker, W. D. Duncan, L. Ferreira, G. C. Hilton, K. D. Irwin, C. D. Reintsema, J. N. Ullom, L. R. Vale, and Y. Xu, *Appl. Phys. Lett.* **85**, 4762 (2004).

⁶J. A. B. Mates, G. C. Hilton, K. D. Irwin, L. R. Vale, and K. W. Lehnert, *Appl. Phys. Lett.* **92**, 023514 (2008).

⁷Y. Nakashima, F. Hirayama, S. Kohjiro, H. Yamamori, S. Nagasawa, A. Sato, S. Yamada, R. Hayakawa, N. Y. Yamasaki, K. Mitsuda, K. Nagayoshi, H. Akamatsu, L. Gottardi, E. Taralli, M. P. Bruijn, M. L. Ridder, J. R. Gao, and J. W. A. den Herder, *Appl. Phys. Lett.* **117**, 122601 (2020).

⁸D. Schwan, P. A. R. Ade, K. Basu, A. N. Bender, F. Bertoldi, H. M. Cho, G. Chon, J. Clarke, M. Dobbs, D. Ferrusca, R. Gusten, N. W. Halverson, W. L. Holzapfel, C. Horellou, D. Johansson, B. R. Johnson, J. Kennedy, Z. Kermish, R. Kneissl, T. Lanting, A. T. Lee, M. Lueker, J. Mehl, K. M. Menten, D. Muders, F. Pacaud, T. Plagge, C. L. Reichardt, P. L. Richards, R. Schaaf, P. Schilke, M. W. Sommer, H. Spieler, C. Tucker, A. Weiss, B. Westbrook, and O. Zahn, *Rev. Sci. Instrum.* **82**, 091301 (2011).

⁹J. Montgomery, A. J. Anderson, J. S. Avva, A. N. Bender, M. A. Dobbs, D. Dutcher, T. Elleflot, A. Foster, J. C. Groh, W. L. Holzapfel, D. Hobe, N. Huang, A. E. Lowitz, G. I. Noble, Z. Pan, A. Rahlin, D. Riebel, G. Smecher, A. Suzuki, and N. Whitehorn, *Proc. SPIE*. **114530X** (2020).

¹⁰G. Signorelli, A. Baldini, C. Bemporad, M. Biasotti, F. Cei, V. Ceriale, D. Corsini, F. Fontanelli, L. Galli, G. Gallucci, F. Gatti, M. Incagli, M. Grassi, D. Nicol, F. Spinella, D. Vaccaro, and M. Venturini, *Nucl. Instrum. Methods Phys. Res.* **824**, 184 (2016).

¹¹A. Tartari, A. Baldini, F. Cei, L. Galli, M. Grassi, D. Nicol, M. Piendibene, F. Spinella, D. Vaccaro, and G. Signorelli, *J. Low Temp. Phys.* **199**, 212 (2020).

¹²G. Jaehnig, K. Arnold, J. Austermann, D. Becker, S. Duff, N. Halverson, M. Hazumi, G. Hilton, J. Hubmayr, A. Lee, M. Link, A. Suzuki, M. Vissers, S. Walker, and B. Westbrook, *J. Low Temp. Phys.* **199**, 646 (2020).

¹³P. R. Roelfsema, H. Shibai, L. Armus, D. Arrazola, M. Audard, M. D. Audley, C. Bradford, I. Charles, P. Dieleman, Y. Doi, L. Duband, M. Eggens, J. Evers, I. Funaki, J. R. Gao, M. Giard, A. di Giorgio, L. M. G. Fernndez, M. Griffin, F. P. Helmich, R. Hijmering, R. Huisman, D. Ishihara, N. Isobe, B. Jackson, H. Jacobs, W. Jellema, I. Kamp, H. Kaneda, M. Kawada, F. Kemper, F. Kerschbaum, P. Khosropanah, K. Kohno, P. P. Kooijman, O. Krause, J. van der Kuur, J. Kwon, W. M. Laauwen, G. de Lange, B. Larsson, D. van Loon, S. C. Madden, H. Matsuhara, F. Najarro, T. Nakagawa, D. Naylor, H. Ogawa, T. Onaka, S. Oyabu, A. Poglitsch, V. Reveret, L. Rodriguez, L. Spinoglio, I. Sakon, Y. Sato, K. Shinozaki, R. Shipman, H. Sugita, T. Suzuki, F. F. S. van der Tak, J. T. Redondo, T. Wada, S. Y. Wang, C. K. Wafelbakker, H. van Weers, S. Withington, B. Vandenbusche, T. Yamada, and I. Yamamura, *Publ. Astron. Soc. Aust.* **35**, e030 (2018).

¹⁴M. D. Audley, G. de Lange, J. R. Gao, B. D. Jackson, R. A. Hijmering, M. L. Ridder, M. P. Bruijn, P. R. Roelfsema, P. A. R. Ade, S. Withington, C. M. Bradford, and N. A. Trappe, *Proc. SPIE*. **107080K** (2018).

¹⁵M. L. Ridder, P. Khosropanah, R. A. Hijmering, T. Suzuki, M. P. Bruijn, H. F. C. Hoovers, J. R. Gao, and M. R. Zuiddam, *J. Low Temp. Phys.* **184**, 60 (2016).

¹⁶M. B. A. J. van der Linden, L. Ferrari, L. Gottardi, J. v. d. Kuur, R. H. d. Hartog, H. Akamatsu, and B. D. Jackson, *J. Low Temp. Phys.* **193**, 661 (2018).

¹⁷Q. Wang, P. Khosropanah, J. van der Kuur, G. de Lange, M. D. A. and A. Aminaei, R. Hijmering, M. L. Ridder, S. Ilyas, A. J. van der Linden, M. P. Bruijn, F. van der Tak, and J. R. Gao, *Rev. Sci. Instrum.* **92**, 014710 (2021).

¹⁸T. Suzuki, P. Khosropanah, M. L. Ridder, R. A. Hijmering, J. R. Gao, H. Akamatsu, L. Gottardi, J. van der Kuur, and B. D. Jackson, *J. Low Temp. Phys.* **184**, 52 (2016).

¹⁹R. Hijmering, R. d. Hartog, M. L. Ridder, A. J. v. d. Linden, J. v. d. Kuur, J. Gao, and B. Jackson, *Proc SPIE*. **99141C** (2016).

²⁰K. Mikko, G. Leif, and S. Hannu, *Supercond. Sci. Technol.* **24**, 049501 (2011).

²¹P. Falferi, M. Bonaldi, M. Cerdonio, A. Vinante, and S. Vitale, *J. Appl. Phys.* **73**, 3589 (1998).

²²M. Audley, Q. Wang, R. Hijmering, P. Khosropanah, G. de Lange, A. J. van der Linden, M. L. Ridder, and E. Taralli, *J. Low Temp. Phys.* **199**, 723

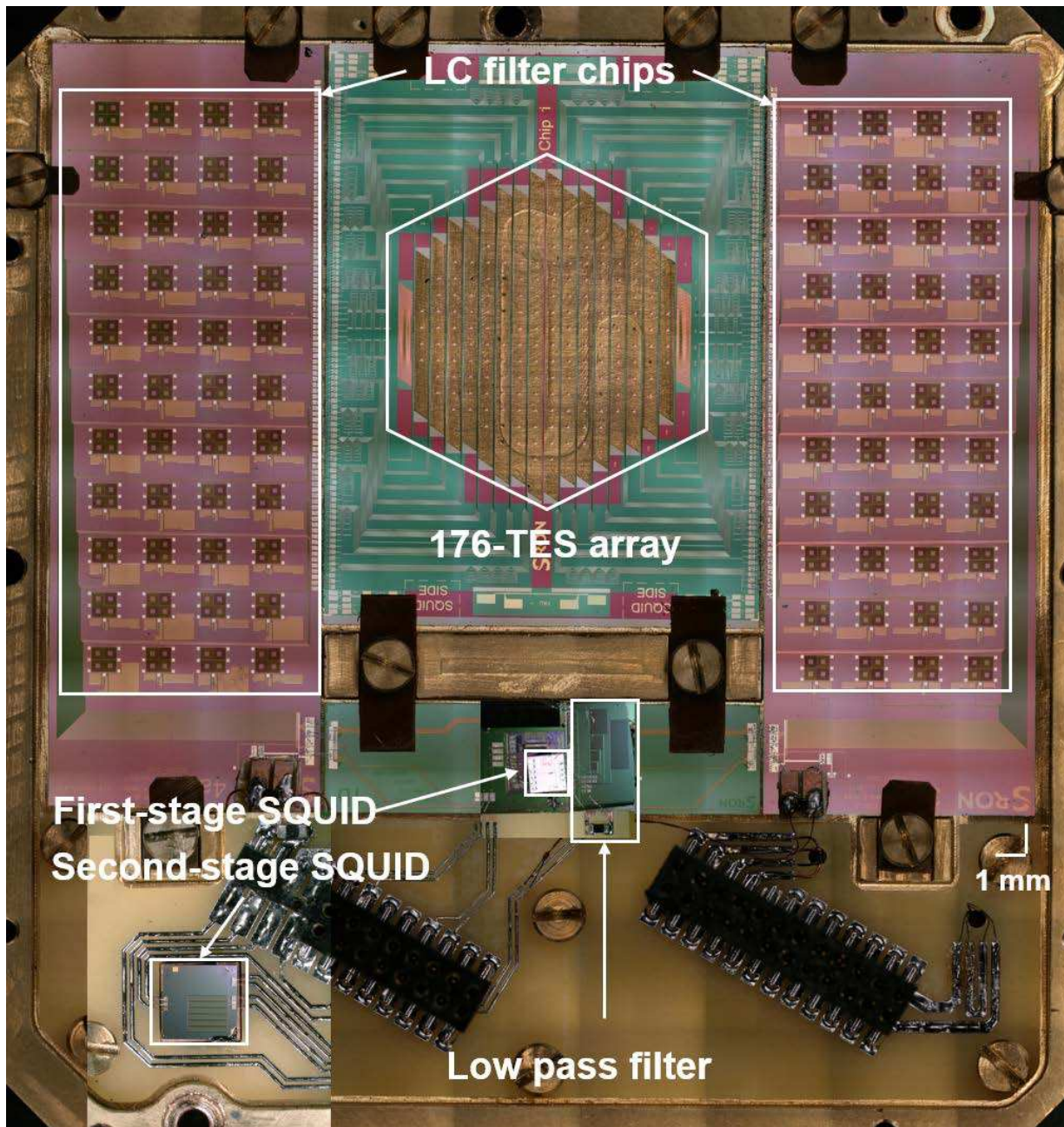
This is the author's peer reviewed, accepted manuscript. However, the online version of record will be different from this version once it has been copyedited and typeset.

PLEASE CITE THIS ARTICLE AS DOI: 10.1063/1.50065570

- (2020).
- ²³Q. Wang, M. Audley, P. Khosropanah, J. v d Kuur, G. de Lange, A. Aminaei, D. Boersma, F. van der Tak, and J. R. Gao, *J. Low Temp. Phys.* **199**, 817 (2020).
- ²⁴(In the wet-etching process we first removed the Si substrate with a KOH solution and further processing is done on the thin Si₃N₄ membrane. We suspect that during the RIE etching of the Si₃N₄ legs also the backside of the legs was attacked by the etching gas leading to changes in surface roughness of the legs which could give additional scattering).
- ²⁵D. J. Goldie, A. V. Velichko, D. M. Glowacka, and S. Withington, *J. Appl. Phys.* **109**, 084507 (2011).
- ²⁶K. Irwin and G. Hilton, Berlin, Heidelberg: Springer **63** (2005).
- ²⁷M. D. Audley, G. de Lange, J.-R. Gao, P. Khosropanah, R. Hijmering, M. Ridder, P. D. Mauskopf, D. Morozov, N. A. Trappe, and S. Doherty, *Rev. Sci. Instrum.* **87**, 043103 (2016).
- ²⁸E. Taralli, P. Khosropanah, L. Gottardi, K. Nagayoshi, M. L. Ridder, M. P. Bruijn, and J. R. Gao, *AIP Adv.* **9**, 045324 (2019).
- ²⁹P. Khosropanah, T. Suzuki, M. L. Ridder, R. A. Hijmering, H. Akamatsu, L. Gottardi, J. van der Kuur, J.-R. Gao, and B. D. Jackson, *Proc SPIE.* **99140B** (2016).

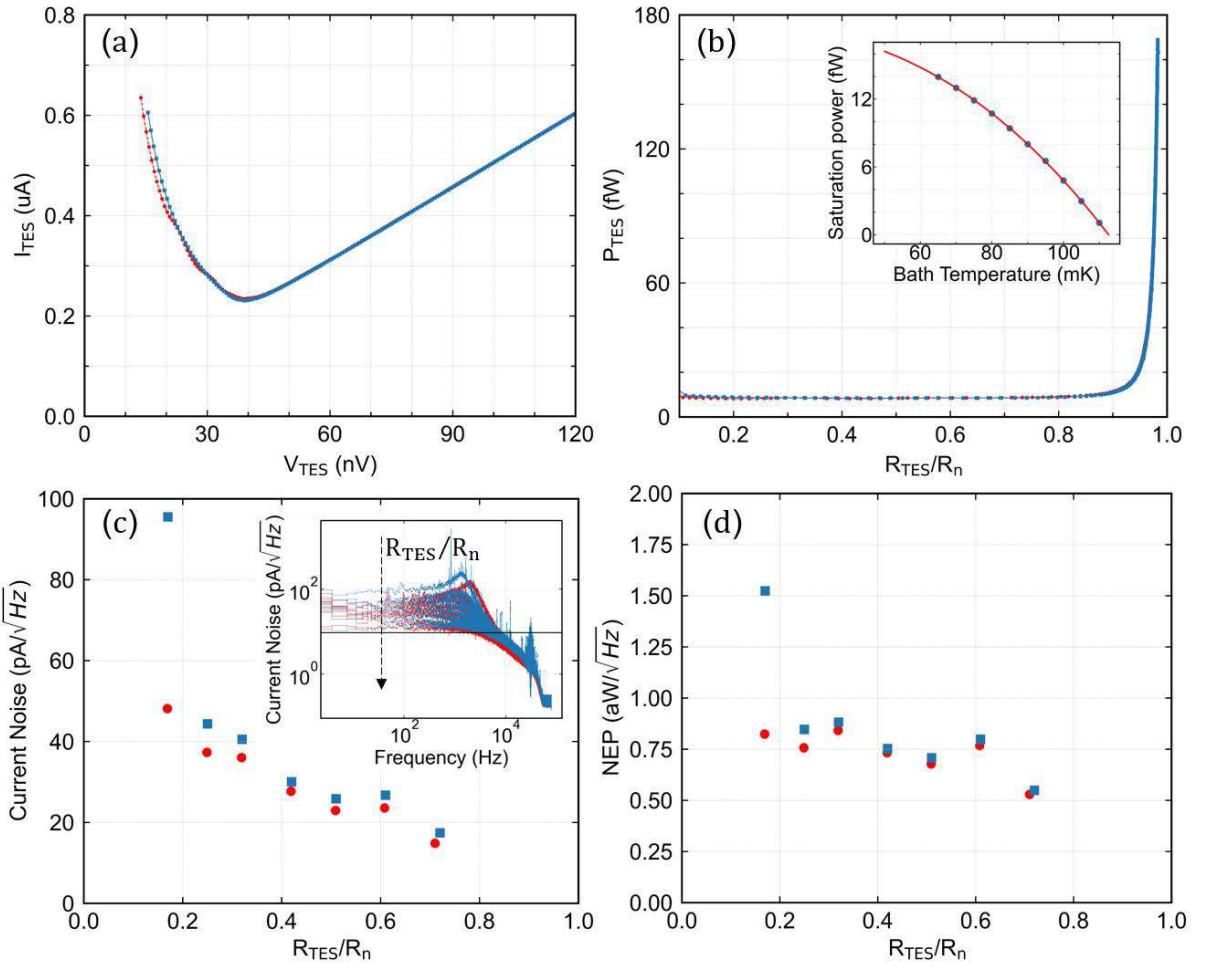
This is the author's peer reviewed, accepted manuscript. However, the online version of record will be different from this version once it has been copyedited and typeset.

PLEASE CITE THIS ARTICLE AS DOI: 10.1063/1.50065570



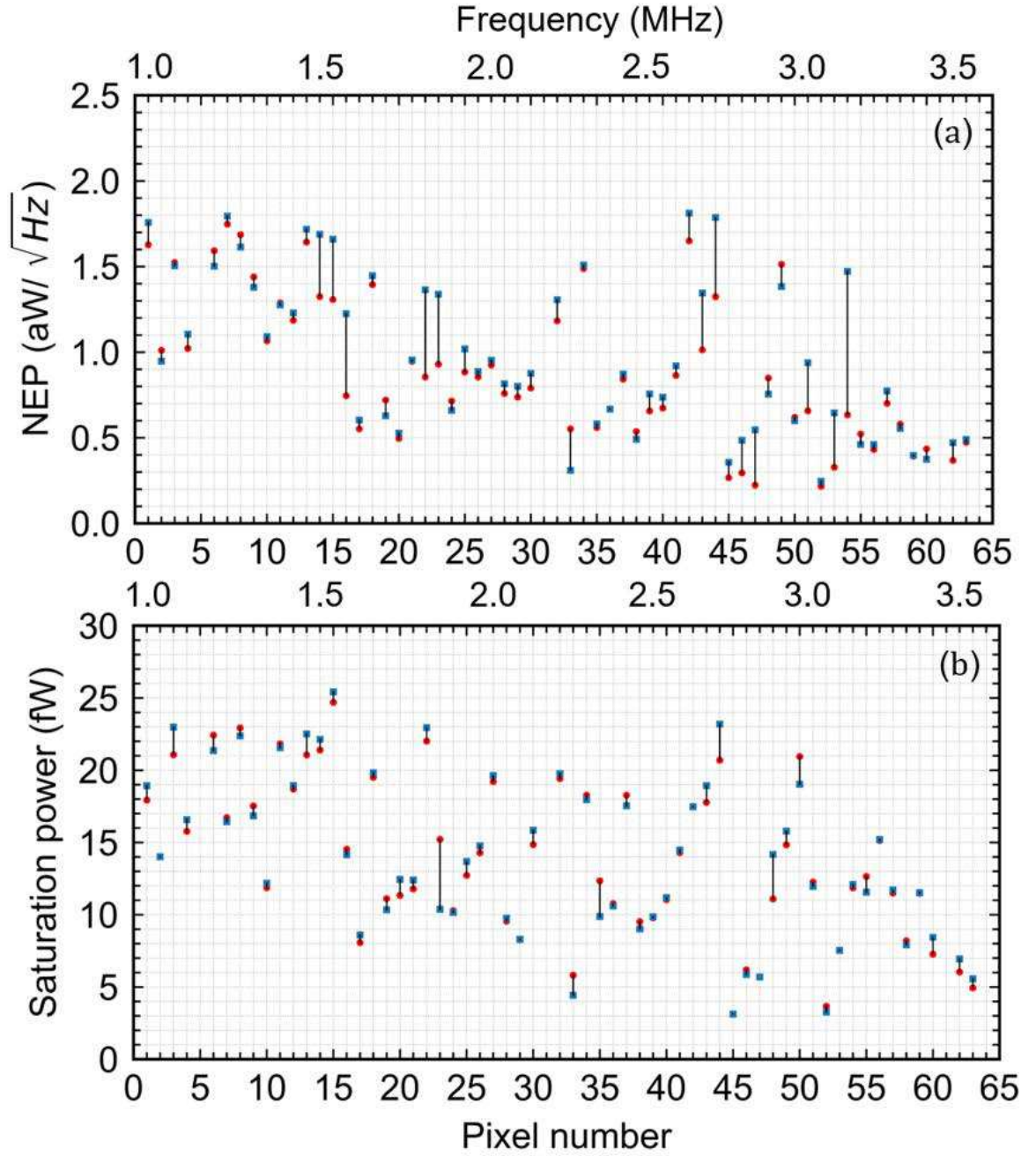
This is the author's peer reviewed, accepted manuscript. However, the online version of record will be different from this version once it has been copyedited and typeset.

PLEASE CITE THIS ARTICLE AS DOI: 10.1063/5.0065570



This is the author's peer reviewed, accepted manuscript. However, the online version of record will be different from this version once it has been copyedited and typeset.

PLEASE CITE THIS ARTICLE AS DOI: 10.1063/1.50065570



This is the author's peer reviewed, accepted manuscript. However, the online version of record will be different from this version once it has been copyedited and typeset.

PLEASE CITE THIS ARTICLE AS DOI: 10.1063/5.0065570

